International Journal of Bifurcation and Chaos, Vol. 29, No. 12 (2019) 1930034 (12 pages)

DOI: 10.1142/S0218127419300349

# Multistability and Bubbling Route to Chaos in a Deterministic Model for Geomagnetic Field Reversals

Paulo C. Rech
*Departamento de Física,*
*Universidade do Estado de Santa Catarina,*
*89219-710 Joinville, Brazil*
*paulo.rech@udesc.br*

Sudarshan Dhua
*School of Sciences, National Institute of Technology,*
*Andhra Pradesh-534102, India*
*sudarshan.math@nitandhra.ac.in*

N. C. Pati*
*Department of Mathematics, The University of Burdwan,*
*Burdwan-713104, West Bengal, India*
*ncpati.math@yahoo.com*

Received March 26, 2019

We report coexisting multiple attractors and birth of chaos via period-bubbling cascades in a model of geomagnetic field reversals. The model system comprises a set of three coupled first-order quadratic nonlinear equations with three control parameters. Up to seven kinds of multistable attractors, viz. fixed point-periodic, fixed point-chaotic, periodic–periodic, periodic-chaotic, chaotic–chaotic, fixed point-periodic–periodic, fixed point-periodic-chaotic are obtained depending on the initial conditions for critical parameter sets. Antimonotonicity is a striking characteristic feature of nonlinear systems through which a full Feigenbaum tree corresponding to creation and annihilation of period-doubling cascades is developed. By analyzing the two-parameters dependent dynamics of the system, a critical biparameter zone is identified, where antimonotonicity comes into existence. The complex dynamical behaviors of the system are explored using phase portraits, bifurcation diagrams, Lyapunov exponents, isoperiodic diagram, and basins of attraction.

*Keywords*: Multistability; antimonotonicity; chaos; geomagnetic field reversals.

## 1. Introduction

Multistability is a striking characteristic feature of many physical systems [Feudel, 2008]. It reveals two or more stable states that coexist for the same values of the system parameters. Exploring multistability is essential as it is not possible to fully determine to which attractor a multistable system will eventually go. Sometimes a topologically nonequivalent attractor is excited if the initial state is perturbed infinitesimally. This unusual behavior has been found in many natural systems and man-made devices (for example, see [Bao *et al.*, 2016;

*Author for correspondence

Gelens *et al.*, 2009; Kengne *et al.*, 2015; Feudel *et al.*, 1996; Li & Sprott, 2013; Feudel & Grebogi, 1997; Wiggers & Rech, 2017; da Silva & Rech, 2018] to mention a few). In contrast to regular systems, since a multistable system exhibits that multiple attractors coexist, it has mutually exclusive basin sets in its basin of attraction. The basin sets of a multistable system are separated by basin boundaries which may have complicated fractal structures [Aguirre *et al.*, 2009].

Period doubling is one of the fundamental routes to chaos in deterministic dissipative systems [Schuster & Just, 2006]. In this scenario, the system undergoes chaos via a sequence of period-doubling bifurcations. In connection with period-doubling bifurcations of unimodal maps, Feigenbaum [Feigenbaum, 1978; Schuster & Just, 2006] showed that the rate of the bifurcations converges to the universal constant $\delta_F = 4.6692\ldots$, known as the Feigenbaum constant. The period-doubling scenario can be observed in systems with at least one control parameter. On the contrary, there are several nonlinear systems exhibiting birth of chaos via concurrent creation and destruction of period-doubling cascades when more than one control parameters are varied simultaneously. This phenomenon is known as antimonotonicity [Dawson *et al.*, 1992] and has been found, both numerically and experimentally, in many physical systems and man-made devices such as Chua's circuit [Kocarev *et al.*, 1993], laser [Lepers *et al.*, 1991], Duffing oscillator [Parlitz & Lauterborn, 1985], jerk systems [Kengne *et al.*, 2017], fractional-order system [Zhang *et al.*, 2018], memristive oscillator [Zhou *et al.*, 2018], ecological models [Vandermeer, 1997] and other nonlinear systems [Newell *et al.*, 1996; Kyprianidis *et al.*, 2000; Bayani *et al.*, 2019], etc. Antimonotonicity shows the birth of chaos via period-bubbling in the nonlinear system.

In this paper, the coexisting multiple attractors, their basin sets structures and antimonotonicity in a deterministic dynamical model for geomagnetic field reversals are investigated. To explore reversals of the Earth's magnetic field, Gissinger [2012] (see also [Gissinger *et al.*, 2010]) framed a simple third-order autonomous nonlinear system given by

$$\left.\begin{aligned}\dot{x} &= \mu x - yz,\\ \dot{y} &= -\nu y + xz,\\ \dot{z} &= \Gamma - z + xy,\end{aligned}\right\} \tag{1}$$

where the state variables $x$, $y$ and $z$ are, respectively, interpreted as the quadrupolar and dipolar components of the magnetic field, and a velocity mode that breaks the mirror symmetry of the Earth core (see [Gissinger, 2012] for details) and $\mu$, $\nu$ and $\Gamma$ are the control parameters.

Obviously, the system (1) is invariant under the transformation: $(x, y, z) \to (-x, -y, z)$. This means that if $(x(t), y(t), z(t))$ is a solution of the system (1) then so is $(-x(t), -y(t), z(t))$. This symmetry could serve a key role in the occurrence of multistable attractors. Dissipation is an essential criterion for a system to support attractors. The general condition for a system to be dissipative is that it has negative flow-divergence in the phase-space. For system (1), the divergence of the flow-field is given by

$$\frac{\partial \dot{x}}{\partial x} + \frac{\partial \dot{y}}{\partial y} + \frac{\partial \dot{z}}{\partial z} = \mu - \nu - 1 \begin{cases} < 0 & \text{if } \mu < 1 + \nu,\\ = 0 & \text{if } \mu = 1 + \nu,\\ > 0 & \text{if } \mu > 1 + \nu. \end{cases}$$

Therefore, the present nonlinear system is dissipative, conservative, or expansive accordingly as $\mu < 1 + \nu$, $\mu = 1 + \nu$, and $\mu > 1 + \nu$. Herein the complex dynamics of the system is explored for non-negative values of the control parameters within the dissipative limit.

For equilibrium solutions, system (1) has a trivial equilibrium point $C_0 = (0, 0, \Gamma)$ and four nontrivial equilibrium points

$$C_{1,2} = \left( \pm\sqrt{\nu + \Gamma\sqrt{\frac{\nu}{\mu}}}, \mp\sqrt{\mu + \Gamma\sqrt{\frac{\mu}{\nu}}}, -\sqrt{\mu\nu} \right),$$

and

$$C_{3,4} = \left( \pm\sqrt{\nu - \Gamma\sqrt{\frac{\nu}{\mu}}}, \pm\sqrt{\mu - \Gamma\sqrt{\frac{\mu}{\nu}}}, \sqrt{\mu\nu} \right).$$

The equilibrium points $C_{3,4}$ emerge if and only if $\Gamma < \sqrt{\mu\nu}$ [Gissinger, 2012]. Therefore, the system has up to five equilibrium points. Moreover, it has three quadratic nonlinear terms and so it is topologically not equivalent to the Lorenz [Lorenz, 1963] and Chen [Chen & Ueta, 1999] systems. The linear stability analysis of system (1) around its equilibrium points and the nature of the bifurcations were

investigated by Elsonbaty and Elsadany [2017]. Some complex behaviors such as crisis-induced intermittency, existence of four-scroll chaotic attractors, etc., of the system were reported by Gissinger [2012]. In this work, the organized structures of the system in the transitional and chaotic regimes are explored. These results provide new insight into the dynamics of flow reversals.

## 2. Long-Term Dynamics of the System

For long-term dynamical behaviors of system (1) and their dependence on the initial states and the control parameters, Eq. (1) is integrated numerically using the fourth-order Runge–Kutta algorithm with a fixed-time step of $10^{-3}$. The solution is then used to obtain the parameter-dependent bifurcation diagrams and the Lyapunov exponents, the two fundamental tools representing the asymptotic behaviors of the system in the transitional and chaotic regimes. All the Lyapunov exponents presented in this paper were computed numerically using Wolf's algorithm [Wolf *et al.*, 1985].

### 2.1. *Coexisting multiple attractors and their basin sets*

In this section, we explore the existence of multistable attractors in system (1) for the following two cases:

***Case I.* $\nu = 0.1$, $\Gamma = 0.1$ and vary $\mu$**

In this case, $\mu$ is considered as the bifurcation parameter varies in the range $0.1 < \mu \leq 0.9$ and the other parameters are fixed as $\nu = \Gamma = 0.1$. Since $(\sqrt{\mu\nu} - \Gamma)$ is positive, all of the five equilibrium points $C_{0,1,2,3,4}$ come into existence. The trivial equilibrium point $C_0$ is unstable with the eigenvalues $\lambda_1 = -1$, $\lambda_{2,3} = -0.05 + 0.5\mu \mp 0.5 \times \sqrt{(\mu - 0.1)(\mu + 0.3)}$, among which $\lambda_{1,2}$ are negative real and $\lambda_3$ is real positive in the chosen parameter space. Bifurcation diagram is a useful tool to identify the dependency of a nonlinear system on its initial states for varying values of control parameters. Figure 1(a) shows the bifurcation diagrams representing variations of local maxima of $z$ of system (1) with respect to the control parameter $\mu \in (0.1, 0.9]$ which is increased/decreased with small equal steps of $5 \times 10^{-4}$. The diagram for increasing $\mu$ is colored in blue and that in red for decreasing $\mu$. Each of the bifurcation diagrams is obtained for varied initial conditions. The final state-space point for every iteration of $\mu$ is taken as the initial condition for the next iteration. The variation of the corresponding largest Lyapunov exponent is shown in Fig. 1(b). These clearly indicate that multistability occurs in system (1) for different values of $\mu$ [see Fig. 2 for enlargement of Fig. 1(a) in different ranges of $\mu$].

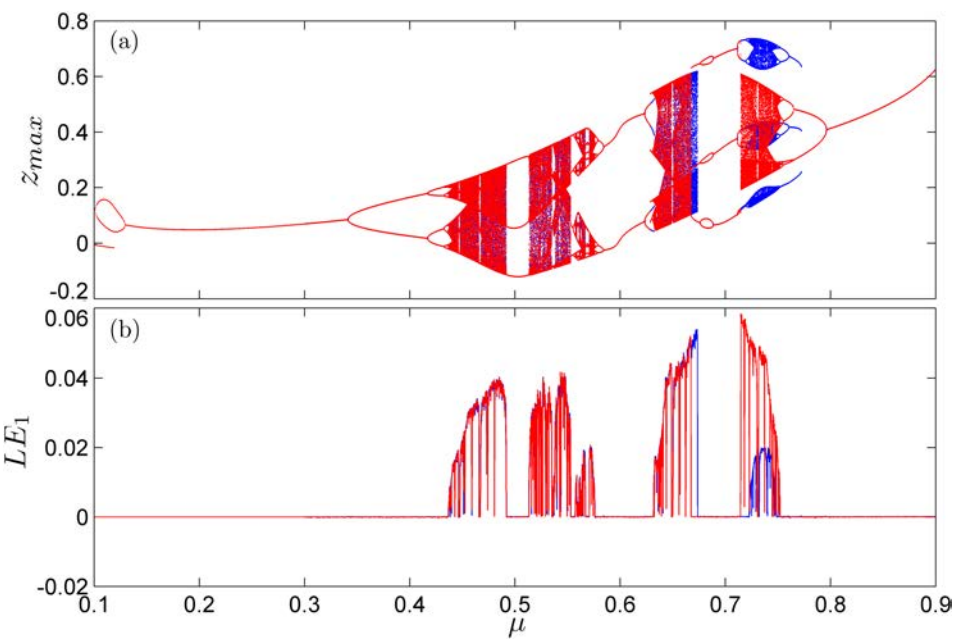


Fig. 1. (a) Bifurcation diagrams for local maxima of $z$ versus the parameter $\mu \in (0.1, 0.9]$ and (b) variation of the corresponding largest Lyapunov exponents for system (1) with $\nu = \Gamma = 0.1$.

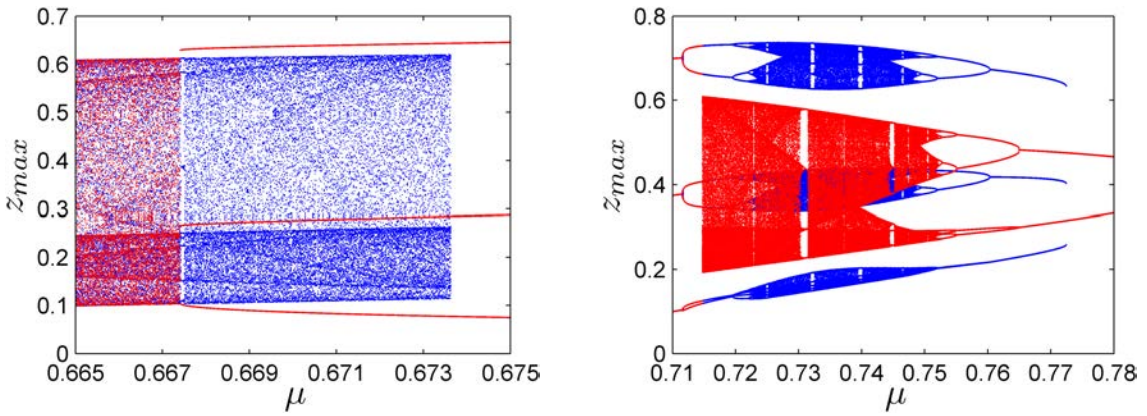


(a) (b)

Fig. 2. Enlargement of Fig. 1(a) in (a) $0.665 \leq \mu \leq 0.675$ and (b) $0.71 \leq \mu \leq 0.78$.

From Fig. 2(a) it follows that in $0.665 \leq \mu \leq 0.675$ when $\mu$ increases, the system evolves in regimes of chaotic motions with an embedded window of periodic oscillation. After that, at $\mu \approx 0.67375$, a period-3 limit cycle attractor is excited via a tangent bifurcation [Schuster & Just, 2006]. Subsequently, the system evolves through the periodic regime if $\mu$ is increased further in the parameter range. By period of a periodic orbit we mean the number of peak amplitudes in the waveform of $z$. Now, if $\mu$ is decreased, the period-3 limit cycle that emerged at $\mu \approx 0.67375$ persists until $\mu$ reaches the critical value $\mu \approx 0.66739$ where the periodic attractor loses its stability to a chaotic attractor. Thus, in the range $0.66739 \lessapprox \mu \lessapprox 0.67375$ the system exhibits hysteresis. In this hysteresis loop one finds the coexistence of periodic and chaotic attractors (see Table 1). Similarly, another hysteresis loop is obtained for $0.71456 \lessapprox \mu \lessapprox 0.77245$. Coexistence of half and full Feigenbaum trees can be observed in this hysteresis loop. Table 1 summarizes that the multistable attractors occur in these hysteretic regions.

### *Case II*. $\mu = 0.08$, $\nu = 0.1$ and vary $\Gamma$

In this case, we fix $\mu = 0.08$, $\nu = 0.1$ and the parameter $\Gamma$ is varied in the range $0.1 \leq \Gamma \leq 0.9$. Since $\sqrt{\mu\nu} \approx 0.089 < \Gamma$, only the three equilibrium points $C_{0,1,2}$ come into existence and the equilibrium point $C_0$ is (locally) spirally stable with one real eigenvalue $\lambda_1 = -1$ and a pair of complex eigenvalues $\lambda_{2,3} = -0.01 \pm \sqrt{(0.09-\Gamma)(0.09+\Gamma)}$. Figure 4 displays the bifurcation diagrams and variation of the corresponding largest Lyapunov exponents as a function of $\Gamma$. As previously, the diagram for increasing $\Gamma$ is colored in blue and that in red for decreasing $\Gamma$. The bifurcation diagram colored in black is obtained for fixed initial conditions $(0.2, 0.2, 0.2)$. From Fig. 4(a) [see also Fig. 5], the system exhibits coexisting fixed point-periodic, fixed point-chaotic, fixed point-periodic–periodic and fixed point-periodic-chaotic

Table 1. Coexisting multiple attractors of system (1) for different values of $\mu$ with $\nu = 0.1$, $\Gamma = 0.1$.

| $\mu$ | Initial Conditions | Attractor Type | Lyapunov Exponents | Ref. |
|---|---|---|---|---|
| 0.67 | $(0, \pm 0.5, 0.1)$<br>$(0, \pm 0.9, 0.1)$ | Left-right spiral chaos<br>Left-right period-3 limit cycles | 0.052, 0, −0.482<br>0, −0.053, −0.377 | Fig. 3(a) |
| 0.735 | $(0, \pm 1.5, 0.1)$<br>$(0, \pm 1, 0.1)$ | Left-right spiral chaos<br>Left-right spiral chaos | 0.046, 0, −0.411<br>0.020, 0, −0.385 | Fig. 3(b) |
| 0.762 | $(0, \pm 1, 0.1)$<br>$(0, \pm 1.5, 0.1)$ | Left-right period-3 limit cycles<br>Left-right period-4 limit cycles | 0, −0.006, −0.332<br>0, −0.032, −0.306 | Fig. 3(c) |
| 0.77 | $(0, \pm 2.5, 0.1)$<br>$(0, \pm 2, 0.1)$ | Left-right period-3 limit cycles<br>Left-right period-2 limit cycles | 0, −0.165, −0.165<br>0, −0.020, −0.310 | Fig. 3(d) |

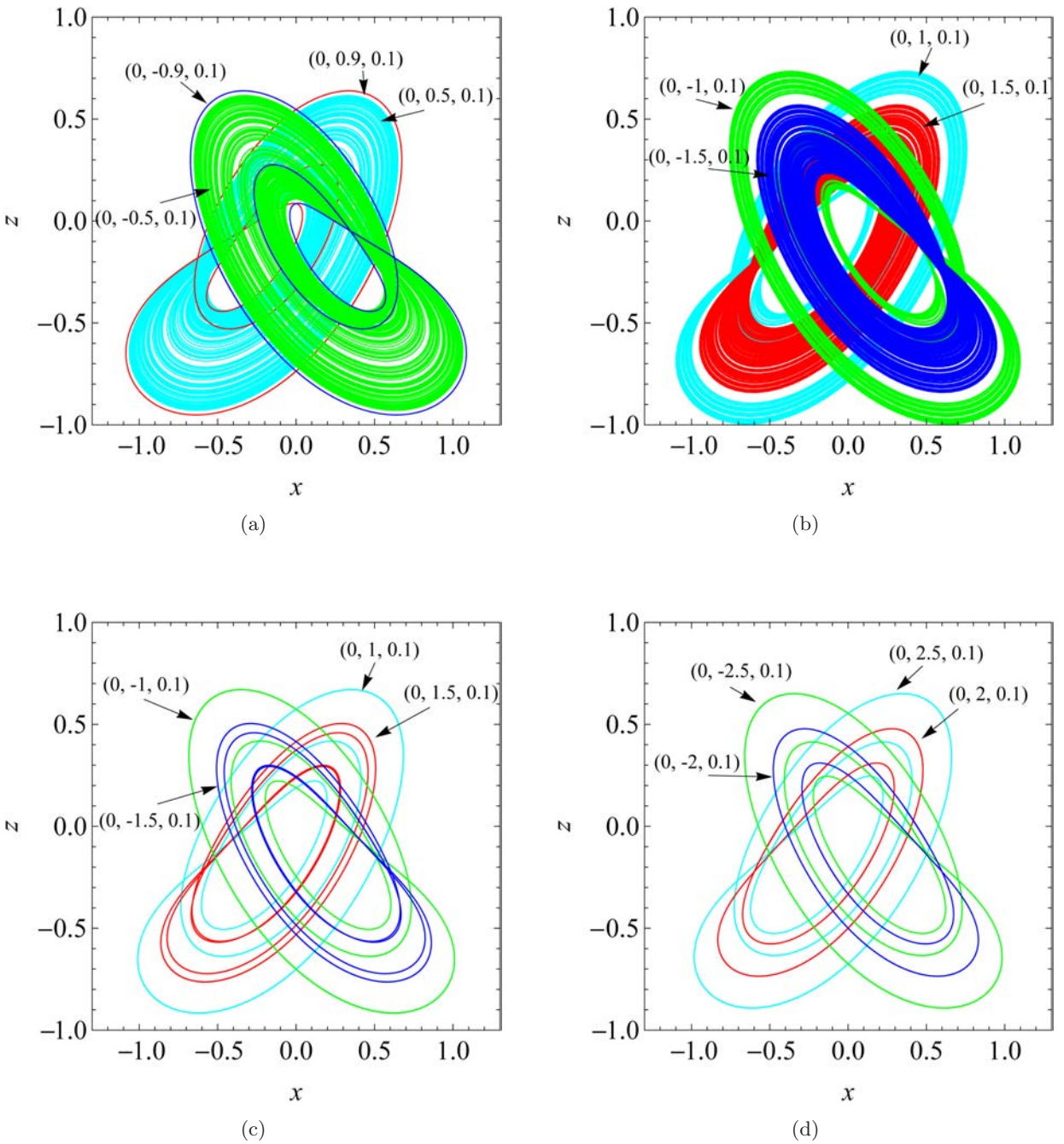


Fig. 3. Phase portraits (projected onto the $xz$-plane) of typical multistable attractors of system (1) for different values of $\mu$ with $\nu = \Gamma = 0.1$: (a) $\mu = 0.67$, (b) $\mu = 0.735$, (c) $\mu = 0.762$ and (d) $\mu = 0.77$.

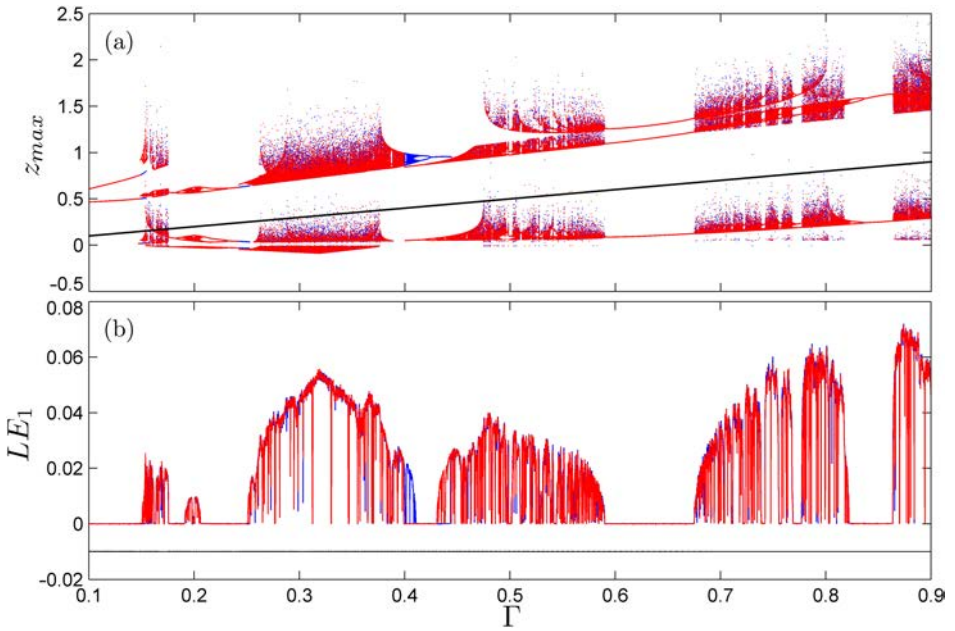


Fig. 4. (a) Bifurcation diagrams for local maxima of $z$ versus the parameter $\Gamma \in [0.1, 0.9]$ and (b) variation of the corresponding largest Lyapunov exponents for system (1) with $\mu = 0.08$ and $\nu = 0.1$.

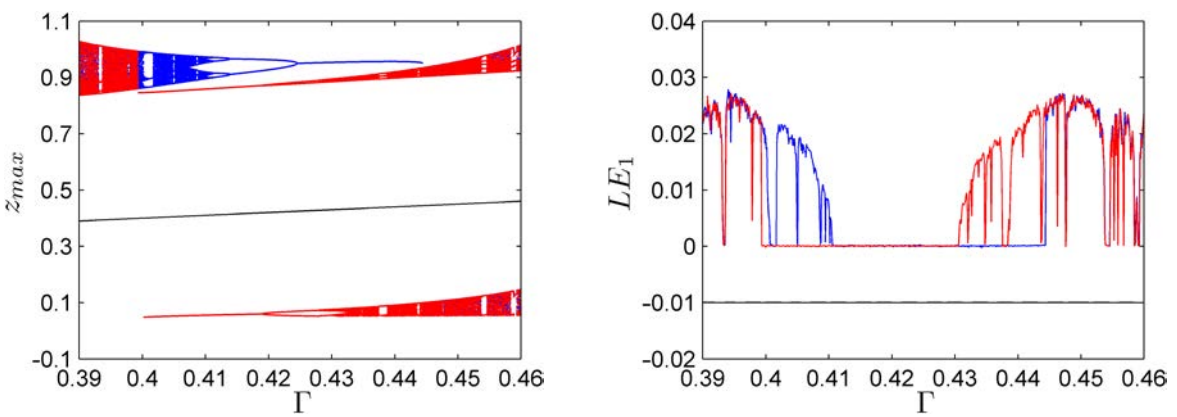


(a) (b)

Fig. 5. Magnification of Fig. 4 in $0.39 \leq \Gamma \leq 0.46$.

Table 2. Coexisting multiple attractors of system (1) for different values of Γ with $\mu = 0.08$ and $\nu = 0.1$.

| Γ | Initial Conditions | Attractor Type | Lyapunov Exponents | Ref. |
|---|---|---|---|---|
| 0.62 | $(0, 0.2, 0.1)$<br>$(0, \pm 2, 0.1)$ | Fixed point attractor<br>Asymmetric period-3 limit cycles | $-0.01$, $-0.01$, $-1.0$<br>0, $-0.03$, $-0.99$ | Fig. 6(a) |
| 0.30 | $(0, 0.2, 0.1)$<br>$(0, \pm 2, 0.1)$ | Fixed point attractor<br>Asymmetric two-scroll chaos | $-0.01$, $-0.01$, $-1$<br>0.046, 0, $-1.066$ | Fig. 6(b) |
| 0.405 | $(0.2, 0.2, 0.2)$<br>$(0.9, -1, 2)$<br>$(2, 1, 2)$ | Fixed point attractor<br>Symmetric period-2 limit cycle<br>Symmetric period-5 limit cycle | $-0.01$, $-0.01$, $-1$<br>0, $-0.274$, $-0.746$<br>0, $-0.002$, $-1.018$ | Fig. 6(c) |
| 0.406 | $(0.2, 0.2, 0.2)$<br>$(0.9, -1, 2)$<br>$(0.9, 0, 2)$ | Fixed point attractor<br>Symmetric period-2 limit cycle<br>Symmetric two-scroll chaos | $-0.01$, $-0.01$, $-1.0$<br>0, $-0.097$, $-0.923$<br>0.018, 0, $-1.038$ | Fig. 6(d) |

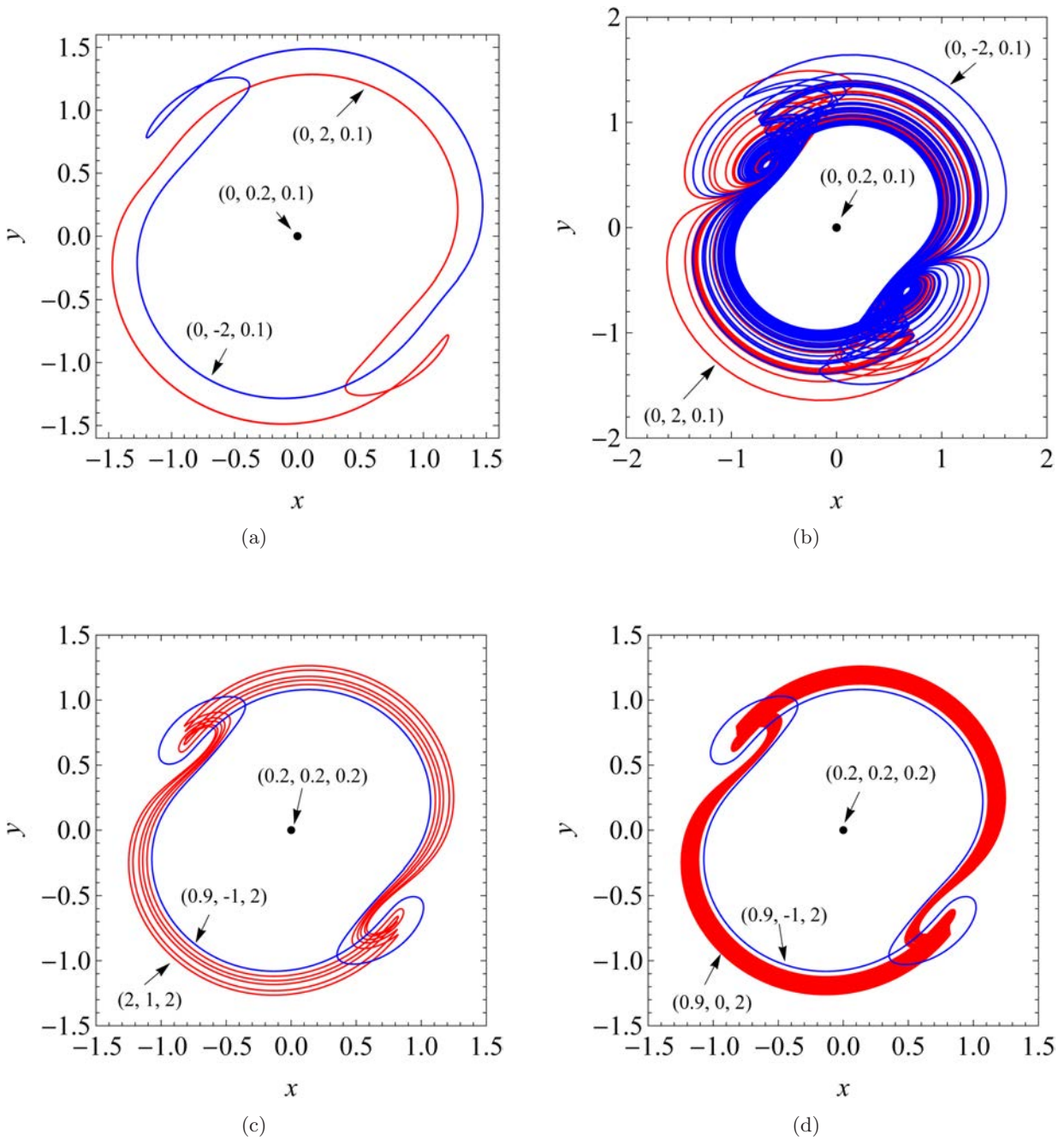


Fig. 6. Phase portraits (projected onto the $xy$-plane) of the coexisting multiple attractors of system (1) for different values of $\Gamma$ with $\nu = 0.1$ and $\mu = 0.08$: (a) $\Gamma = 0.62$, (b) $\Gamma = 0.30$, (c) $\Gamma = 0.405$ and (d) $\Gamma = 0.406$.

attractors for different values of Γ as summarized in Table 2.

The basins of attraction for the coexisting multiple attractors are shown in Fig. 7 where the basin sets of different attractors are marked in different colors. Figure 7(a) shows the basin sets for coexisting period-3 and double-scroll chaotic attractors at $\mu = 0.67, \nu = \Gamma = 0.1$, Fig. 7(b) displays the basin sets for fixed point-periodic coexisting attractors at $(\mu, \nu, \Gamma) = (0.08, 0.1, 0.62)$, and Fig. 7(c) represents

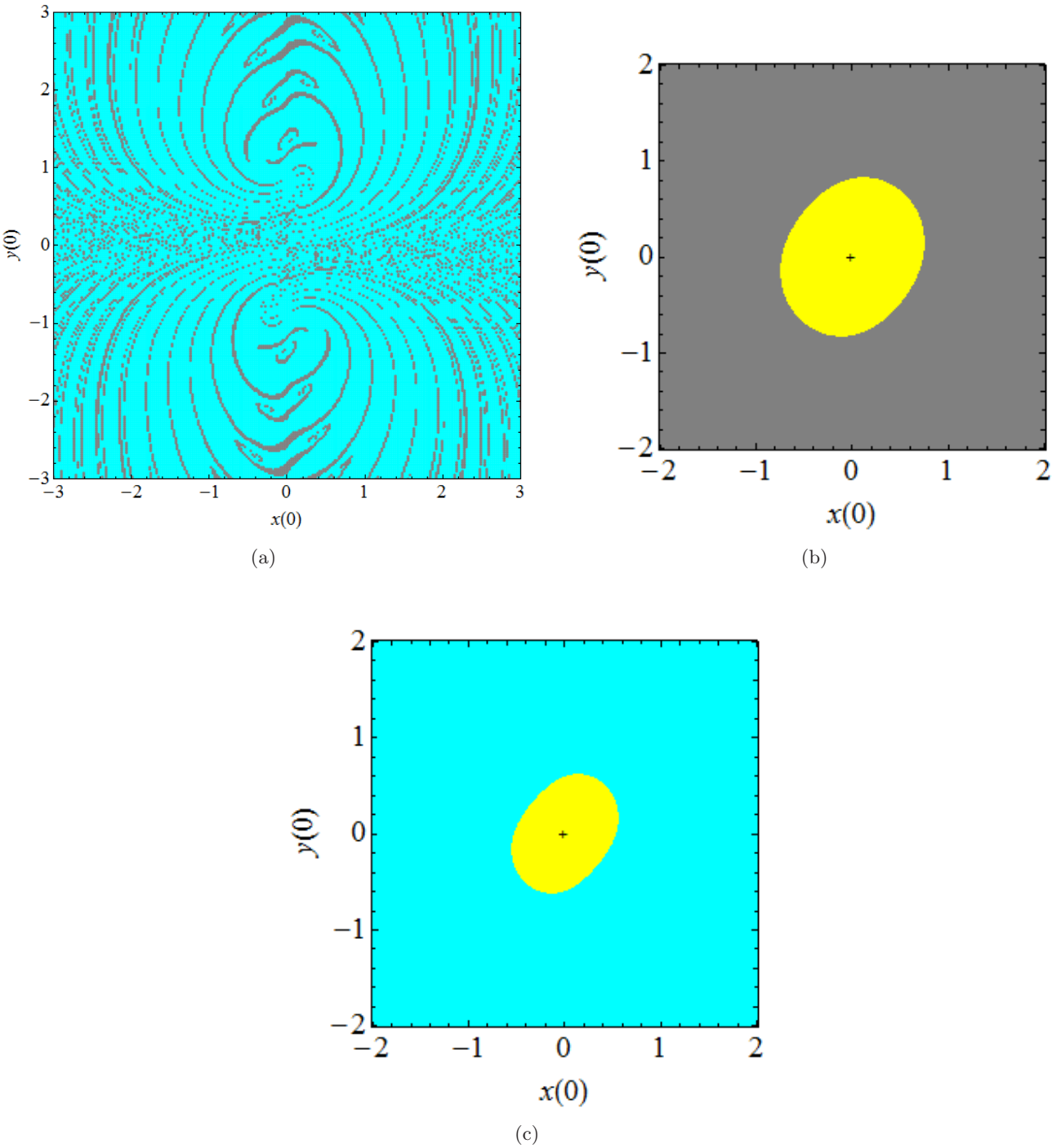


Fig. 7. Cross-section of the attractor basins with $z(0) = 0$ for different values of $\mu$ and Γ with $\nu = 0.1$: (a) $(\mu, \Gamma) = (0.67, 0.1)$, gray region represents the basin set of period-3 limit cycles and cyan region for the chaotic attractors, (b) $(\mu, \Gamma) = (0.08, 0.62)$, yellow region is the basin set of the fixed point attractor and gray region is associated with the limit cycles and (c) $(\mu, \Gamma) = (0.08, 0.3)$, yellow region is the basin set of the fixed point attractor and cyan region is the basin set of the chaotic attractors.

the basin sets for coexisting fixed point-chaotic attractors at $(\mu, \nu, \Gamma) = (0.08, 0.1, 0.30)$. Note that the basin boundaries in Figs. 7(b) and 7(c) are closed curves.

## 3. Period-Bubbling Transition to Chaos

So far we have investigated the asymptotic behaviors of the system (1) when only one control parameter is varied. In order to explore more complex behaviors of the system, we shall now study the dynamics subject to variation of two control parameters. Figure 8 represents the asymptotic behaviors of system (1) in terms of the two leading Lyapunov exponents in the biparameter space $(\mu, \Gamma) \in [0.64, 0.74] \times [0.111, 0.123]$ for fixed initial conditions $(x(0), y(0), z(0)) = (2, 2, 2)$ and $\nu = 0.1$.

From Fig. 8, one observes the occurrence of chaotic motions delimited on both sides by periodic oscillations, a typical characteristic feature of antimonotonicity. Bifurcation diagrams for $z_{\max}$, local maxima of $z$, in terms of $\mu \in [0.64, 0.74]$ are presented in Fig. 9 for some discrete values of $\Gamma$ in the range $0.111 \leq \Gamma \leq 0.123$. These clearly show transition to chaos via period-bubbling. For example, when $\Gamma = 0.135$, the system exhibits period-2 solution in $0.64 \leq \mu \leq 0.74$. Period-doubling bubbles occur when $\Gamma$ decreases smoothly. In this process a period-4 bubble is obtained when, for example, $\Gamma = 0.123$ [see Fig. 9(a)], period-8 bubble at $\Gamma = 0.121$ [see Fig. 9(b)], period-16 bubble at $\Gamma = 0.1206$ [see Fig. 9(c)], period-32 bubble at $\Gamma = 0.1205$ [see Fig. 9(d)] and so on. Upon further decrease in $\Gamma$, this period-doubling process continues until chaos delimited on both sides by infinite period-doubling trees [see Figs. 9(e) and 9(f)] emerges at $\Gamma \approx 0.120435$. The role of the two control parameters $\mu$ and $\Gamma$ on the emergence of the period-bubbling are illustrated in Fig. 10 in terms of the isoperiodic diagram.

We shall now calculate the convergence rate $\delta_n = (\mu_{n-1} - \mu_n)/(\mu_n - \mu_{n+1})$, $n = 2, 3, 4, \ldots$, of the period-doubling/period-halving bifurcations near the development of the full Feigenbaum tree, $\mu_n$ being the value of $\mu$ at the onset of period-$2^n$ cascade. In connection with the development of such Feigenbaum cascades, Oppo and Politi [1984] showed that the period-doubling/period-halving bifurcations convergence rate $\delta_n$ slows down and converges to the square root of the Feigenbaum constant $\delta_F = 4.6692\ldots$ when chaos delimited on both sides by infinite period-doubling cascades disappears. For the present nonlinear system, the convergence rate (see Fig. 11) is calculated up to the first five period-doubling cascades in the antimonotonicity region and is found to be in good agreement with the scaling property of Oppo and Politi [1984].

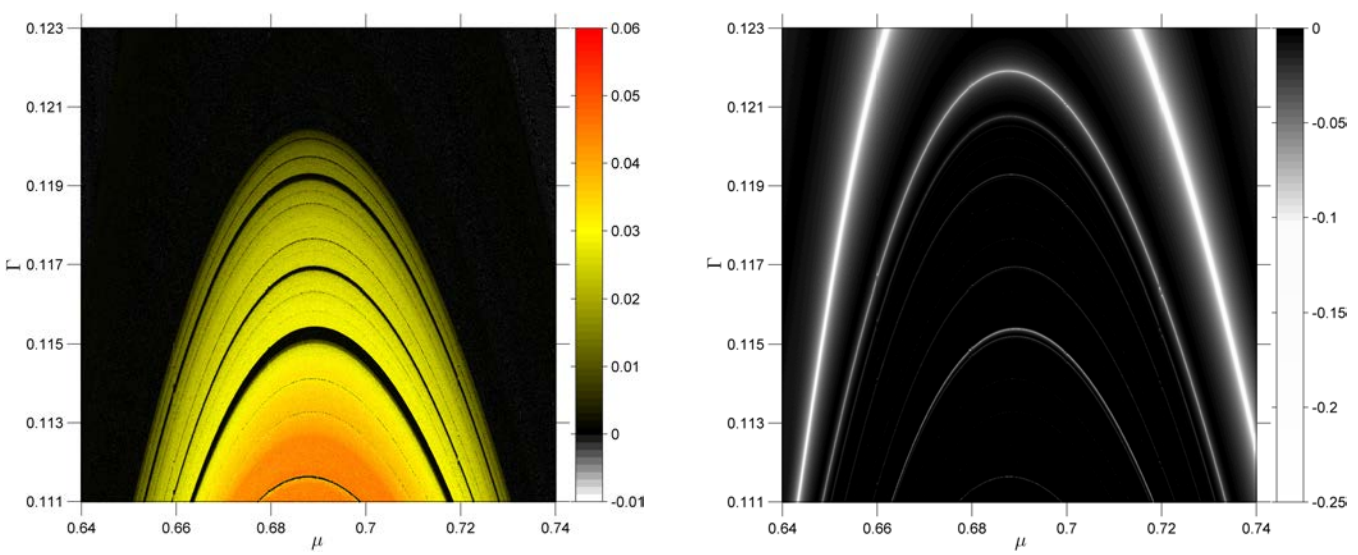


(a) (b)

Fig. 8. Variation of the two leading Lyapunov exponents $LE_{1,2}(LE_1 \geq LE_2)$ [(a) $LE_1$ and (b) $LE_2$] of system (1) in the biparameter space $(\mu, \Gamma) \in [0.64, 0.74] \times [0.111, 0.123]$ with $\nu = 0.1$. The color bars represent the color codes of the numerical values of the Lyapunov exponents.

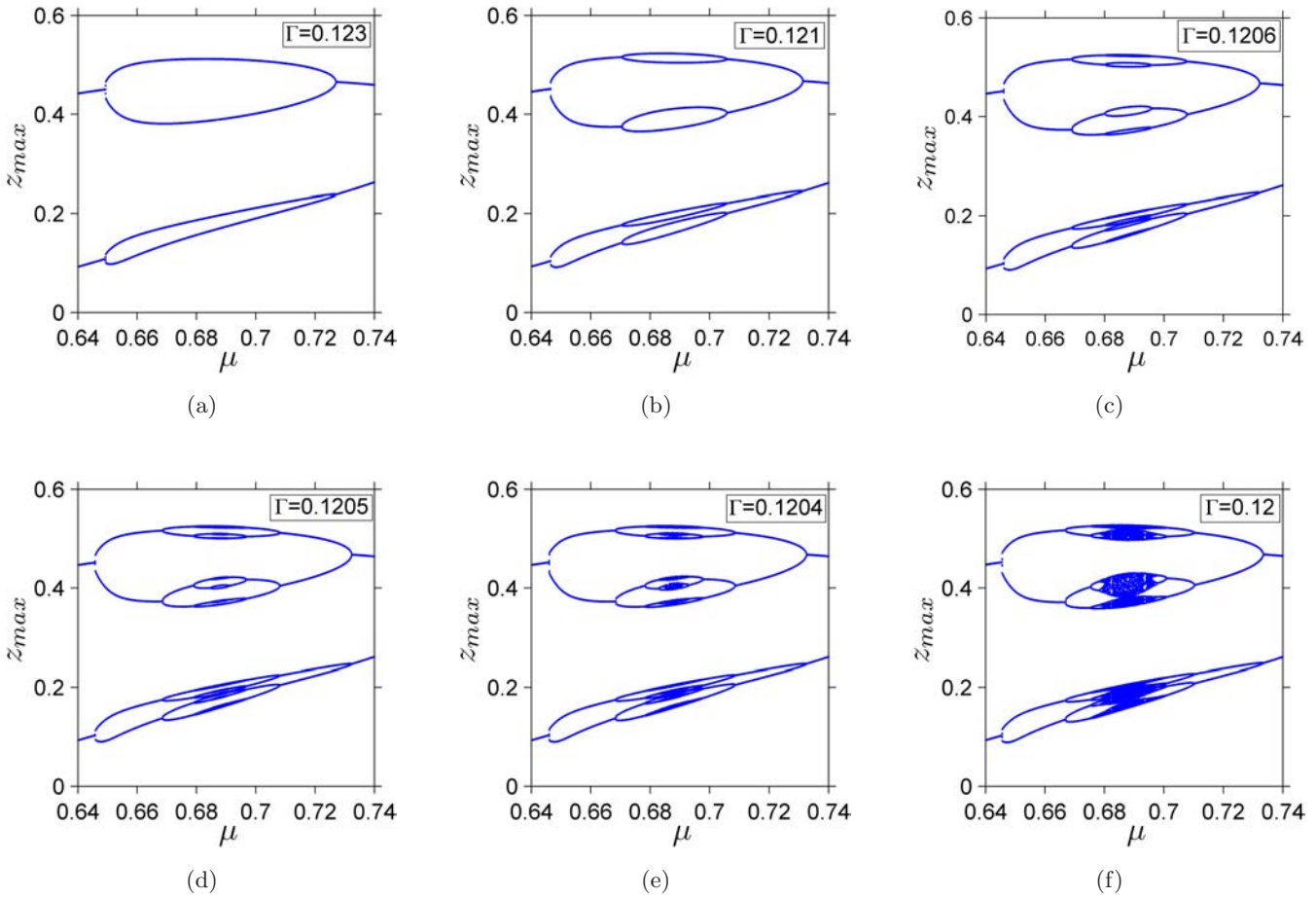


Fig. 9. Onset of chaos via period-bubbling cascades: (a) period-4 bubble at $\Gamma = 0.123$, (b) period-8 bubble at $\Gamma = 0.121$, (c) period-16 bubbles at $\Gamma = 0.1206$, (d) period-32 bubbles at $\Gamma = 0.1205$, (e) and (f) chaos delimited on both sides by period-doubling cascades at $\Gamma = 0.1204$ and $\Gamma = 0.12$, respectively.

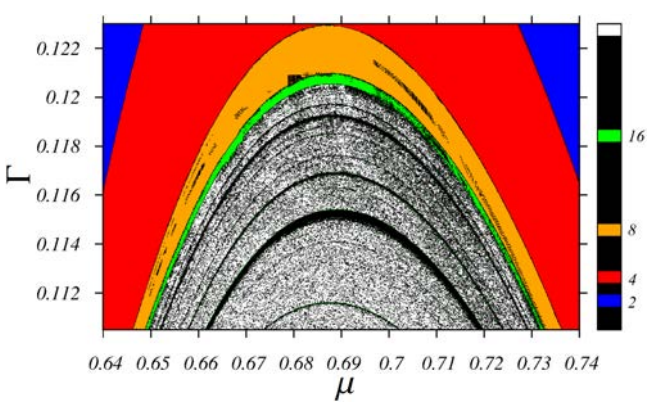


Fig. 10. $\mu$ versus $\Gamma$ parametric diagram in the occurrence of the period-bubbling. The color bar represents the periods of the periodic regions.

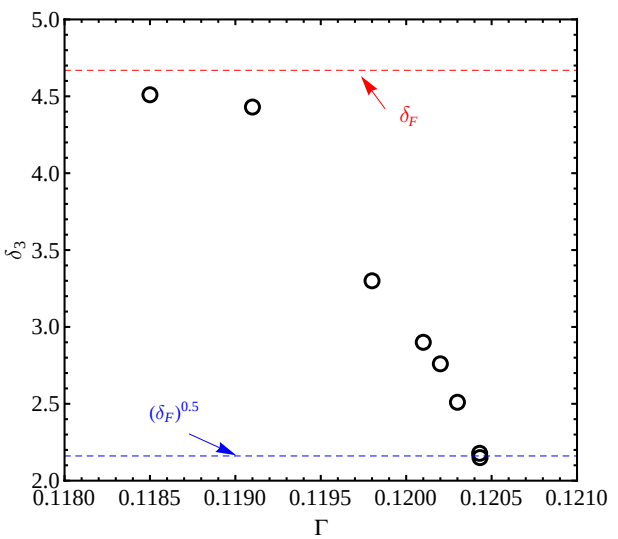


Fig. 11. Convergence rate of the third approximation, $\delta_3$, of the Feigenbaum ratio for the period-doubling bifurcations near the onset of the full Feigenbaum tree of system (1).

## 4. Summary and Conclusions

In this paper, we have investigated the complex dynamical behaviors of a flow reversals model. Studies reveal that the system exhibits up to seven different types of coexisting multiple attractors in its parameter space. The complexity of the multistable attractors is analyzed by using their basin sets. For some coexisting attractors, the basin boundaries are closed curves. Also, the system exhibits chaos via period-bubbling mechanism. Finally, the results presented in this paper can be useful to understand the complicated behaviors of flow reversals of many physical systems.

## Acknowledgments

N. C. Pati acknowledges the financial support received from CSIR, New Delhi, India. P. C. Rech thanks Conselho Nacional de Desenvolvimento Científico e Tecnológico-CNPq, and Fundação de Amparo à Pesquisa e Inovação do Estado de Santa Catarina-FAPESC, Brazilian Agencies, for financial support.

## References

Aguirre, J., Viana, R. L. & Sanjuán, M. A. F. [2009] "Fractal structures in nonlinear dynamics," *Rev. Mod. Phys.* **81**, 333–386.

Bao, B. C., Li, Q. D., Wang, N. & Xu, Q. [2016] "Multistability in Chua's circuit with two stable node-foci," *Chaos* **26**, 043111.

Bayani, A., Rajagopal, K., Khalaf, A. J. M., Jafari, S., Leutcho, G. & Kengne, J. [2019] "Dynamical analysis of a new multistable chaotic system with hidden attractor: Antimonotonicity, coexisting multiple attractors, and offset boosting," *Phys. Lett. A* **383**, 1450–1456.

Chen, G. & Ueta, T. [1999] "Yet another chaotic attractor," *Int. J. Bifurcation and Chaos* **9**, 1465–1466.

da Silva, A. & Rech, P. C. [2018] "Numerical investigation concerning the dynamics in parameter planes of the Ehrhard–Muller system," *Chaos Solit. Fract.* **110**, 152–157.

Dawson, S. P., Grebogi, C., Yorke, J. A., Kan, I. & Koçak, H. [1992] "Antimonotonicity: Inevitable reversals of period-doubling cascades," *Phys. Lett. A* **162**, 249–254.

Elsonbaty, A. & Elsadany, A. [2017] "Bifurcation analysis of chaotic geomagnetic field model," *Chaos Solit. Fract.* **103**, 325–335.

Feigenbaum, M. J. [1978] "Quantitative universality for a class of nonlinear transformations," *J. Stat. Phys.* **19**, 25–52.

Feudel, U., Grebogi, C., Hunt, B. R. & Yorke, J. A. [1996] "Map with more than 100 coexisting low-period periodic attractors," *Phys. Rev. E* **54**, 71–81.

Feudel, U. & Grebogi, C. [1997] "Multistability and the control of complexity," *Chaos* **7**, 597–604.

Feudel, U. [2008] "Complex dynamics in multistable systems," *Int. J. Bifurcation and Chaos* **18**, 1607–1626.

Gelens, L., Beri, S., Van der Sande, G., Mezosi, G., Sorel, M., Danckaert, J. & Verschaffelt, G. [2009] "Exploring multistability in semiconductor ring lasers: Theory and experiment," *Phys. Rev. Lett.* **102**, 193904.

Gissinger, C., Dormy, E. & Fauve, S. [2010] "Morphology of field reversals in turbulent dynamos," *Europhys. Lett.* **90**, 49001.

Gissinger, C. [2012] "A new deterministic model for chaotic reversals," *Eur. Phys. J. B* **85**, 137.

Kengne, J., Njitacke Tabekoueng, Z., Kamdoum Tamba, V. & Nguomkam Negou, A. [2015] "Periodicity, chaos, and multiple attractors in a memristor-based Shinriki's circuit," *Chaos* **25**, 103126.

Kengne, J., Negou, A. N. & Tchiotsop, D. [2017] "Antimonotonicity, chaos and multiple attractors in a novel autonomous memristor-based jerk circuit," *Nonlin. Dyn.* **88**, 2589–2608.

Kocarev, L., Halle, K. S., Eckert, K. & Chua, L. O. [1993] "Experimental observation of antimonotonicity in Chua's circuit," *Int. J. Bifurcation and Chaos* **3**, 1051–1055.

Kyprianidis, I. M., Stouboulos, I. N., Haralabidis, P. & Bountis, T. [2000] "Antimonotonicity and chaotic dynamics in a fourth-order autonomous nonlinear electric circuit," *Int. J. Bifurcation and Chaos* **10**, 1903–1915.

Lepers, C., Legrand, J. & Glorieux, P. [1991] "Experimental investigation of the collision of Feigenbaum cascades in lasers," *Phys. Rev. A* **43**, 2573–2575.

Li, C. & Sprott, J. C. [2013] "Multistability in a butterfly flow," *Int. J. Bifurcation and Chaos* **23**, 1350199-1–10.

Lorenz, E. N. [1963] "Deterministic nonperiodic flow," *J. Atmos. Sci.* **20**, 130–141.

Newell, T. C., Kovanis, V., Gavrielides, A. & Bennett, P. [1996] "Observation of the concurrent creation and annihilation of periodic orbits in a nonlinear RLC circuit," *Phys. Rev. E* **54**, 3581–3590.

Oppo, G. L. & Politi, A. [1984] "Collision of Feigenbaum cascades," *Phys. Rev. A* **30**, 435–441.

Parlitz, U. & Lauterborn, W. [1985] "Superstructure in the bifurcation set of the Duffing equation $\ddot{x} + d\dot{x} + x + x^3 = f\cos(\omega t)$," *Phys. Lett. A* **107**, 351–355.

Schuster, H. G. & Just, W. [2006] *Deterministic Chaos*: *An Introduction* (John Wiley & Sons).

Vandermeer, J. [1997] "Period 'bubbling' in simple ecological models: Pattern and chaos formation in a quartic model," *Ecol. Model.* **95**, 311–317.

Wiggers, V. & Rech, P. C. [2017] "Multistability and organization of periodicity in a van der Pol–Duffing oscillator," *Chaos Solit. Fract.* **103**, 632–637.

Wolf, A., Swift, J. B., Swinney, H. L. & Vastano, J. A. [1985] "Determining Lyapunov exponents from a time series," *Physica D* **16**, 285–317.

Zhang, S., Zeng, Y., Li, Z. & Zhou, C. [2018] "Hidden extreme multistability, antimonotonicity and offset boosting control in a novel fractional-order hyperchaotic system without equilibrium," *Int. J. Bifurcation and Chaos* **28**, 1850167-1–18.

Zhou, L., Wang, C., Zhang, X. & Yao, W. [2018] "Various attractors, coexisting attractors and antimonotonicity in a simple fourth-order memristive Twin-T oscillator," *Int. J. Bifurcation and Chaos* **28**, 1850050-1–18.